Multi-frequency Polarimetric Change Analysis for Agricultural Monitoring

Alberto Alonso-Gonzalez[a] and Konstantinos P. Papathanassiou[a]
[a]German Aerospace Center (DLR), Microwaves and Radar Institute, Muenchener Strasse 20, 82234 Wessling

Abstract

This work analyzes the changes on the Polarimetric SAR response obtained over agricultural fields for different types of crops during its phenological evolution. A Polarimetric Change Analysis technique will be employed which is based on the optimization of the polarimetric contrast in order to extract information related to both, the intensity and the type of change. Particular attention will be given to how the phenological changes are perceived by the different frequencies, including L-, C- and X-band. For this analysis the DLR's F-SAR CROPEX 2014 campaign will be used, containing fully polarimetric SAR data at these 3 frequencies.

1 Introduction

During the last years, space-borne SAR systems performed time series of acquisitions of the same scene at different time instants. Moreover, this tendency is expected to increase in the next years due to the availability of sensors that are strongly oriented towards systematic and repeated acquisitions. These datasets provide information related to the scene and to its temporal evolution, making them very valuable for the analysis of dynamic effects.

For the exploitation of time series change detection and interpretation is essential. Change detection techniques have been employed to detect and localize the changes between SAR acquisitions. In this work, a Polarimetric SAR (PolSAR) change analysis will be employed [4], which describes not only the amount but also the type of change, helping to understand the observed changes and the scene evolution.

SAR sensors are sensitive to geometric and dielectric properties of the scatterers within vegetated scenario. When dealing with multi-frequency acquisitions it is important to notice that both of these properties are frequency dependent and, therefore, the observed changes will be different depending on the wavelength. This paper analyzes which are the main detectable phenological changes over agricultural fields that may be monitored with PolSAR data and how they are observed by the different frequencies.

2 Polarimetric change analysis

PolSAR systems measure the complex reflectivity of the scene employing different polarization states for the transmitted and received radar echoes. Usually the orthogonal vertical and horizontal linear polarizations are employed. Then, the information measured by the radar may be represented by the scattering matrix $\mathbf{S}$, which is usually vectorized into the scattering vector $\mathbf{k}$. In the Pauli basis, this vector may be expressed as [5]

$$\mathbf{k} = \frac{1}{\sqrt{2}} \left[S_{hh} + S_{vv}, S_{hh} - S_{vv}, S_{hv} + S_{vh}\right]^T \quad (1)$$

where S_{ij} represents the measured scattering coefficient for the $i, j \in [h, v]$ transmitted and received polarization.

Under the assumption of distributed scatterers, the PolSAR response of a target may be completely characterized by the second order statistics of the measured scattering vector $\mathbf{k}$, provided by the scattering covariance matrix, which may be estimated as [6]

$$\mathbf{Z} = \langle \mathbf{k}\mathbf{k}^H \rangle_n = \frac{1}{n} \sum_{i=1}^{n} \mathbf{k}_i \mathbf{k}_i^H \quad (2)$$

where $\mathbf{k}_i$ represents the scattering vector of the *i*-th pixel, as defined in (1), and n represents the number of (independent) pixels averaged.

The polarimetric change between two acquisitions, characterized by $\mathbf{Z}_1$ and $\mathbf{Z}_2$ polarimetric responses, may be obtained by exploiting the differences between covariance matrices. In [7] the polarimetric contrast measure was introduced, in order to describe the relative change of the backscattered power at each polarization state $\mathbf{w}$

$$P_c(\mathbf{Z}_1, \mathbf{Z}_2, \mathbf{w}) = \frac{\mathbf{w}^H \mathbf{Z}_2 \mathbf{w}}{\mathbf{w}^H \mathbf{Z}_1 \mathbf{w}}. \quad (3)$$

A polarimetric change analysis has been proposed based on this concept in [4][2]. The generalized eigendecomposition of $\mathbf{Z}_1$ and $\mathbf{Z}_2$ matrices is employed to extract the range of values of the polarimetric contrast and the corresponding polarization states $\mathbf{w}$ that produce them. Additionally, a change representation is proposed for an easy interpretation of the observed changes. This representation separates the observed changes into an increase and a decrease of the polarimetric contrast, and depicts the polarization

states that produce the change in two Pauli RGB images

$$\mathbf{p}_{inc} = 10\left[\sum_{i|\lambda_i>1}^{p}\left(\log_{10}\lambda_i\mathbf{p}_i\right)^2\right]^{\frac{1}{2}} \quad (4)$$

$$\mathbf{p}_{dec} = 10\left[\sum_{i|\lambda_i<1}^{p}\left(-\log_{10}\lambda_i\mathbf{p}_i\right)^2\right]^{\frac{1}{2}}, \quad (5)$$

where $\mathbf{p}_{inc}$ and $\mathbf{p}_{dec}$ stand for the Pauli RGB polarimetric change representation of the increase and decrease, respectively, λ_i represent the generalized eigenvalues and $\mathbf{p}_i = \left[|w_i^1|, |w_i^2|, |w_i^3|\right]^T$ is the Pauli representation of the generalized eigenvectors, as described in [4][2].

In order to visualize the detected changes among all the acquisitions, the polarimetric *change matrices* may be employed. The axis of these matrices are the dates of the different acquisitions. For each combination of acquisition pairs (i, j), in the upper diagonal the $\mathbf{p}_{inc}$ representation between the i and j acquisitions is shown, whereas in the lower diagonal (j, i) the $\mathbf{p}_{dec}$ between i and j is displayed.

3 Results

For the analysis and interpretation of the described polarimetric change analysis, data acquired in the frame of the CROPEX 2014 campaign are used. This campaign consists of different acquisitions by DLR's F-SAR airborne sensor, from the end of May to the beginning of August 2014, over the Wallerfing agricultural test-site, in southern Germany. The campaign covers most of the growing season of different types of crops as maize, wheat and barley. Several multi-baseline acquisitions were performed during these dates, acquiring fully-polarimetric and interferometric data with different baselines at L-, C- and X-band. Some ground pictures of the different where ground measurements were taken crops are shown in Fig. 1.

Fig. 2a shows the change matrices for maize crops at L-, C- and X-band. The plant growing process is clearly observed as an increase mostly in green and red colors, corresponding to volume and double bounce components in the Pauli RGB representation. This growing process is also visible on the ground pictures on Figs. 1h - 1k. As it may be seen, the change is visible at all frequencies. However, the temporal span of the detected change (visible mainly on the vertical span over the change matrix) is shorter for higher frequencies. This is related to the limitation in terms of penetration to the ground, which limits the visibility of the latter stages of the growing period. At higher frequencies, when the penetration to the ground level is lost, only the upper part of the plant is observed and even if there is plant growth it is not detected as a change since the same upper portion of the canopy is only observed.

However, the variability induced by observing the same processes at different frequencies is not only related to distinct canopy penetration. Different wavelengths are sensitive to distinct types of scatterers within the plant. Figs. 2b and 2c show the change matrices for barley and wheat crops, respectively, at L-, C- and X-band. In this case three

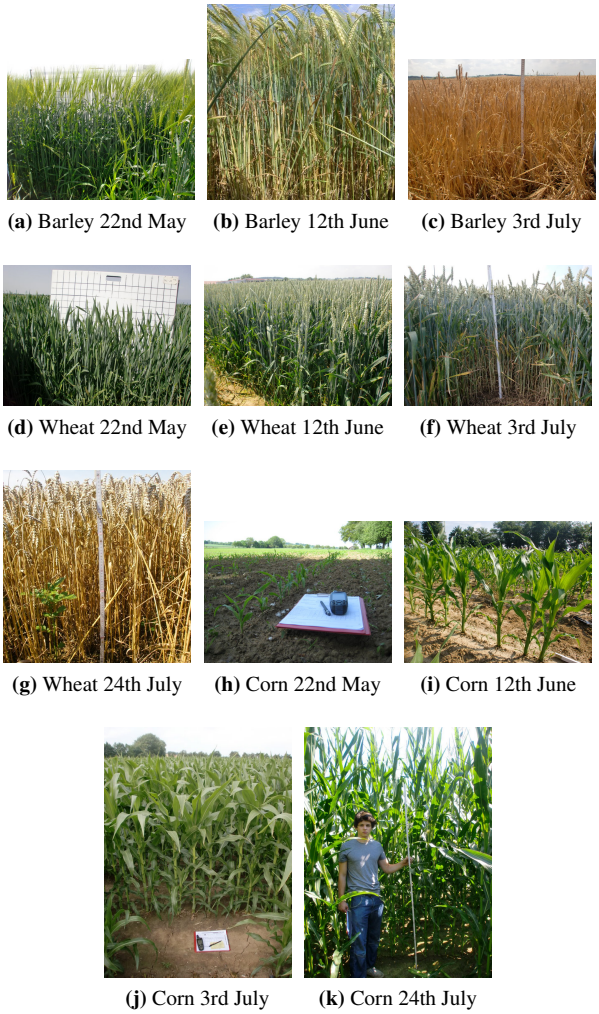

(a) Barley 22nd May **(b)** Barley 12th June **(c)** Barley 3rd July

(d) Wheat 22nd May **(e)** Wheat 12th June **(f)** Wheat 3rd July

(g) Wheat 24th July **(h)** Corn 22nd May **(i)** Corn 12th June

(j) Corn 3rd July **(k)** Corn 24th July

Figure 1 Pictures of the crops at different dates during the acquisition campaign.

different phenological changes may be observed: the fruit maturation, plant drying or senescence and the harvest of the crops, which are marked with blue, orange and purple polygons, respectively, in Figs. 2b and 2c. When comparing the change matrices at the three frequencies some significant differences that might not be explained in terms of canopy penetration start to appear. The fruit maturation, for instance, appears as a clear increase in C- and X-band but it is totally invisible at L-band. During this process, significant changes are occurring at the head of the plants, where the fruit develops and some spikes are grown. This changes are clearly visible at C- and X-band, with wavelengths of 9cm and 3cm, respectively, but invisible at L-band since the wavelength (23cm) is too large to properly interact with these smaller scatterers.

After the fruit maturation, the plant drying and senescence occurs. It may be seen on the ground pictures in Figs. 1a - 1c and in Figs. 1e - 1g. This phenological change is characterized by a significant decrease in terms of vegetation water content over the plants, which is translated into a dielectric change on the plant canopy. The plant drying process is observed as a decrease in L- and C-band but not visible at X-band. This may be related to the limited pen-

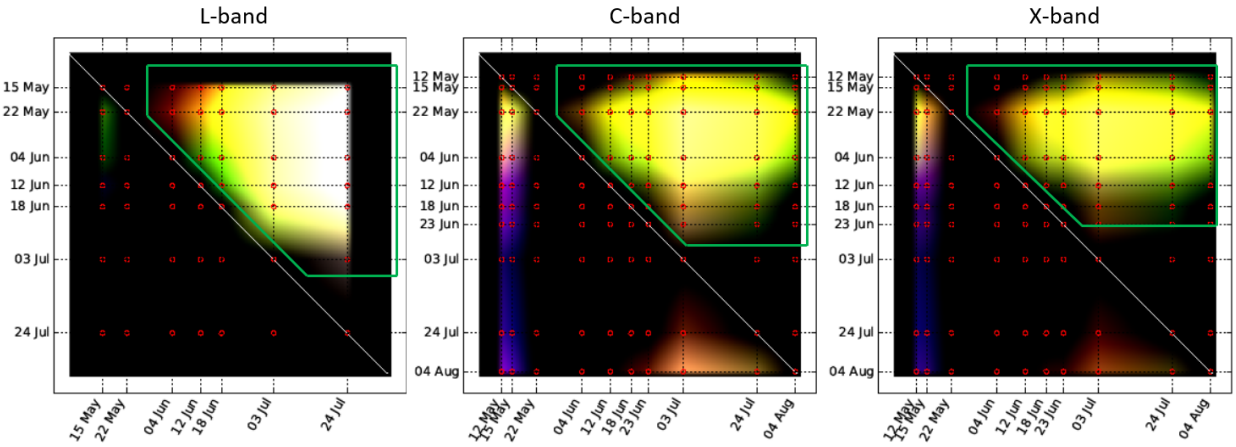

(a) Maize

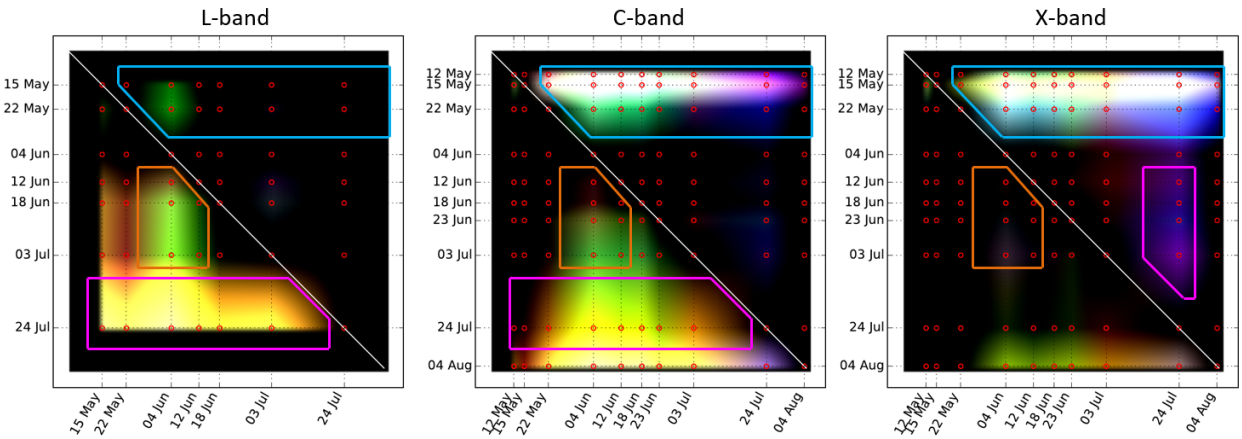

(b) Barley

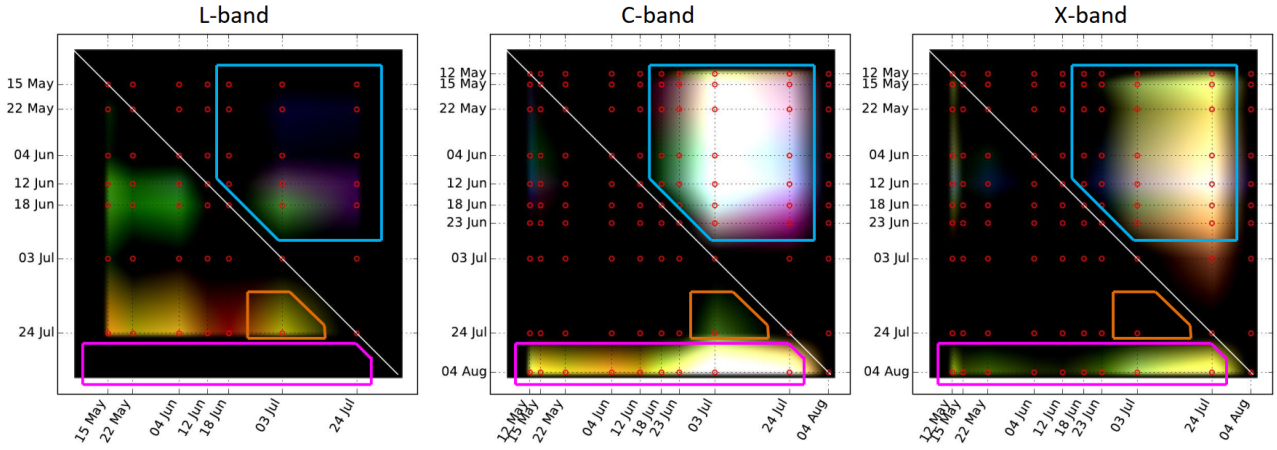

(c) Wheat

Figure 2 Change matrices for different crops at different frequencies. Upper diagonal represents the increasing while the lower diagonal represents the decreasing polarization states in Pauli RGB. The polygons indicate the phenological changes: plant growing in green, fruit maturation in blue, plant drying and senescence in orange and harvest in purple.

etration into the canopy at X-band in order to observe this decrease.

Finally, when the crop is harvested, most of the plant canopy is removed from the field, although the lower part of the stalks usually remains. This change is observed as a decrease in L- and C-band, as it may be expected. However, at X-band an increase is observed, mainly appearing in blue color in Fig. 2b. This change represents the increase of the ground scattering component. This is especially visible at higher frequencies, where the ground was strongly attenuated or not visible before the harvest due the high extinction through the canopy. However, on the wheat crops,

shown in Fig. 2c, this change appears also as a decrease at X-band. Therefore, the observation of these changes at different frequencies is dependent on the crop type.

4 Sensitivity analysis

This section defines a lower bound for the sensitivity of the previously mentioned polarimetric change analysis technique with respect to the Equivalent Number of Looks (ENL). The statistics of generalized eigenvalues and eigenvectors have not been analyzed in the literature but, as mentioned in [4], the generalized eigenvalue problem of two positive definite covariance matrices $\mathbf{A}$ and $\mathbf{B}$ is equivalent to the classical eigenvalue problem of the $\mathbf{A}^{-1}\mathbf{B}$ matrix. In the change detection context, the statistics of the complex Hotelling–Lawley trace τ_{HLT}, i.e. $\mathrm{tr}(\mathbf{A}^{-1}\mathbf{B})$, were analyzed in [1], where analytical expressions for its first statistical moments were defined:

$$\mu_{HLT} = \frac{pN}{Q} \tag{6}$$

$$m^2_{HLT} = \frac{N^2}{Q^3 - Q}\left(p^2\left(Q + \frac{1}{N}\right) + p\left(\frac{Q}{N} + 1\right)\right) \tag{7}$$

where N corresponds to the ENL, p is the matrix dimension (3 for monostatic full-pol and 2 for dual-pol) and $Q = N - p$.
With this information the variance $\sigma^2_{\tau_{HLT}} = m^2_{HLT} - \mu^2_{HLT}$ may be obtained. Although this information cannot be directly related to the individual generalized eigenvalues, the standard deviation $\sigma_{\tau_{HLT}}$ gives an idea of the variability of the generalized eigenvalues λ_i in the presence of speckle noise, as $\mathrm{tr}(\mathbf{A}^{-1}\mathbf{B}) = \sum_i \lambda_i$. Therefore we will use $\sigma_{\tau_{HLT}}$ to approximate the sensitivity of the polarimetric change analysis technique as a function of the ENL, by considering that only changes larger than $\sigma_{\tau_{HLT}}$ may be detected. It is worth noticing that this is like a worst case scenario since the changes might also be visible at other polarization states than those with maximum noise variability. The minimum detectable change, according to this assumption, may be seen in Fig. 3 for full- and dual-pol cases.

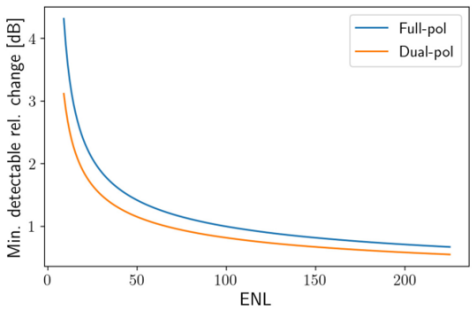

Figure 3 Minimum detectable change vs ENL for full- and dual-pol data.

When looking at Fig. 3 it may be seen that dual-pol is able to detect changes around 0.25 dB smaller than full-pol. This is related to the fact that, since the covariance matrix is smaller, a better estimation may be achieved by the same number of independent samples. One may wrongly conclude that dual-pol is more sensitive to polarimetric changes than full-pol, however, it is worth noticing here that full-pol has a larger space for the polarimetric optimization and a larger contrast is expected than in dual-pol for the same change.

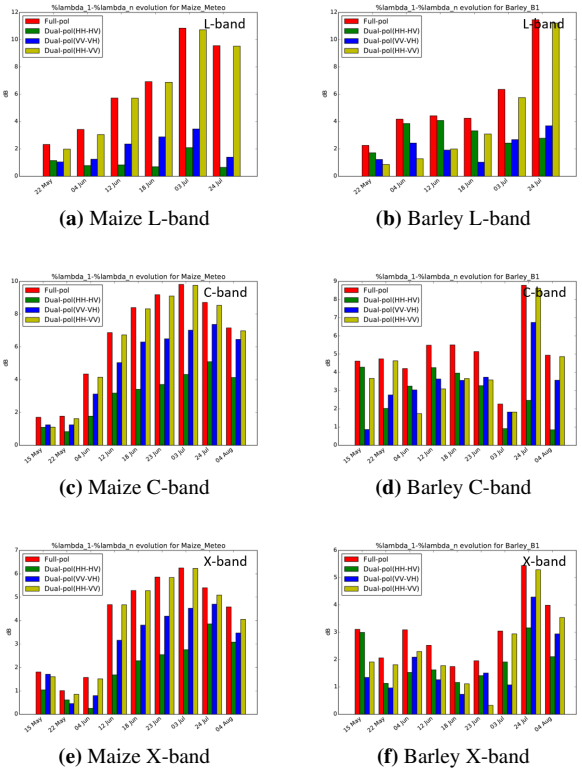

(a) Maize L-band **(b)** Barley L-band

(c) Maize C-band **(d)** Barley C-band

(e) Maize X-band **(f)** Barley X-band

Figure 4 Range of values of the polarimetric contrast (difference between max. and min. contrast in dB) between the first image and the rest of the time series for different frequencies and polarimetric configurations.

To analyze the observed range of values of the polarimetric contrast, the difference between the maximum and minimum contrast in dB is shown in Fig. 4 for maize and barley fields, for different frequencies and also for distinct full- and dual-pol configurations. In this case the change between the first acquisition and the rest of the time series is shown, which corresponds to the first line/column of the change matrices shown in Figs. 2a - 2c. The range of values of full-pol is represented by the red bar while HH-HV, VV-VH and HH-VV configurations are represented in green, blue and yellow colors, respectively. It may be clearly seen that the red bar in Fig. 4 presents always the larger contrast, as expected. Dual-pol configurations have significantly less contrast, especially co and cross-pol configurations, in red and blue colors. The HH-VV dual-pol, in yellow, is sometimes close to full-pol in terms of contrast but this configuration is usually not available as it requires the transmission of two pulses by the radar. This is related to the ability to measure the correlation between the two co-pol channels which is generally non negligi-

ble and has a significant information in terms of physical interpretation [5]. It is worth noticing here that the difference between full- and dual-pol is most of the times significantly larger than the 0.25 dB sensitivity difference shown in Fig. 3, which confirms that full-pol will effectively have better sensitivity to detect changes.

Comparing the different frequencies in Fig. 4 it may be seen how larger contrast values are generally obtained for lower frequencies (note that the vertical axis is different for each plot). This means that generally there is a larger polarimetric diversity along the phenological evolution of the crops observed at L-band than at C-band than at X-band, respectively.

5 Complementarity of interferometry

Interestingly, the monitoring of the previously mentioned phenological changes may be complemented by using interferometry, as already shown in [3][9]. Geometric and dielectric changes occurring during the crop evolution have also an effect on the radar vertical reflectivity profile and, therefore, the interferometric coherence and phase are also affected. The interferometric phase center height evolution from TanDEM-X [8] long-baseline acquisitions was analyzed in [3] over the same testsite during the next year (2015). However, similar crop evolution has been measured for maize, barley and wheat crops on both years. The observed evolution of the interferometric phase center height for these three crops is shown in Fig. 5.

As it may be seen in Fig. 5a, the effect of the maize growing process is clearly observed as an increase on the phase center height from June to August. It is worth noticing that due to the relatively large extinction through the canopy at X-band, this growth is clearly reflected into the interferometric phase. In the polarimetric change analysis in Fig. 2a, the sensitivity to the growing process at X-band was lost after the middle of June, due to the limited penetration to the ground, which results into observing only the upper part of the canopy and no subsequent changes in terms of polarimetry. Here, interferometry can fill this gap by observing the increase of the phase center height, as seen in Fig. 5a. However, the measured phase center height at September was around 1.5m while the ground measured plant height was around 3m, which indicates that there is some degree of penetration in the upper part of the canopy, which is also less dense, as it may be seen in Fig. 1k.

For barley and wheat crops, as seen in Figs. 5b and 5c, a decreasing interferometric phase center height is observed. These crops were already grown at the beginning of the campaign and the observed phenological changes are the fruit maturation, plant drying and harvest, as shown in Figs. 2b and 2c. No significant change during the fruit maturation is observed in Fig. 5, but the plant drying process is clearly reflected as a decrease in the interferometric phase center height. Indeed, when comparing the trends in Figs. 5b and 5c with the Vegetation Water Content (VWC) measured from ground, shown in Figs. 6a and 6b, a good correspondence may be seen. It is worth noticing that this

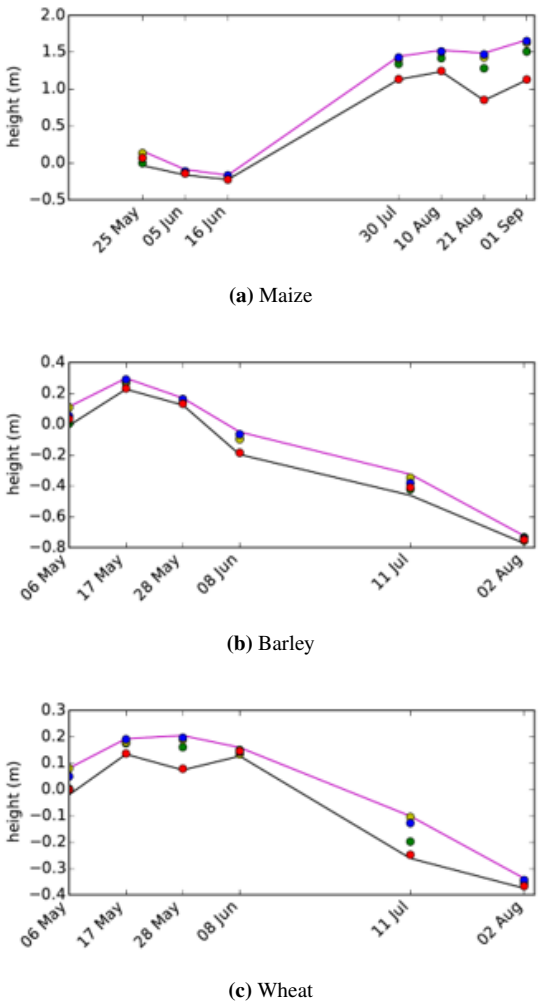

(a) Maize

(b) Barley

(c) Wheat

Figure 5 TanDEM-X Interferometric phase center height evolution for different crops, from [3].

particular change, the plant drying and senescence, was not visible on the polarimetric change analysis for X-band, in Figs. 2b and 2c, while it becomes clear on the interferometric phase center height evolution. This is a good example of the complementarity between polarimetric and interferometric observables for crop pheological evolution characterization. It also shows how dielectric changes on the plant canopy affect the observed interferometric phase.

6 Conclusions

The polarimetric change analysis technique [4] can be employed to detect different types of phenological changes over crops, like the seedbed preparation, plant growing, fruit maturation, plant drying or senescence and harvest. However, the visibility of these changes for each crop type depends on the observing frequency. Longer wavelengths like L-band have better penetration into the canopy and, therefore, they have better visibility of the growing process for large or dense crops like maize. On the other hand, some changes during fruit maturation occurring on the head of the plant for some cereals like wheat and barley are only visible at C- and X-band since these struc-

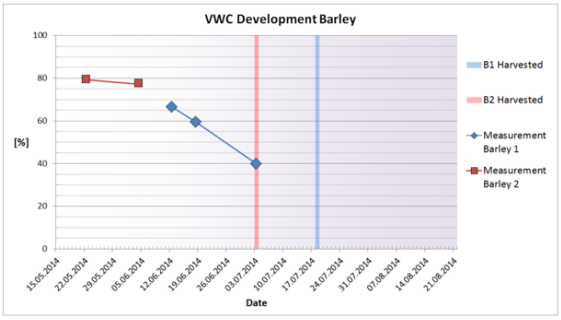

(a) Barley

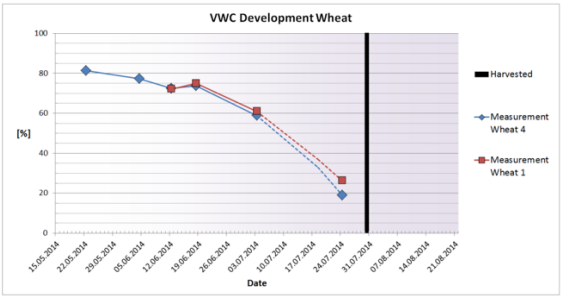

(b) Wheat

Figure 6 Vegetation Water Content evolution measured for barley and wheat crops.

tures are too small to properly interact with longer wavelengths. Therefore a multi-frequency approach can benefit significantly from this in order to increase the sensitivity to the different changes, but also for the interpretation of the observed changes, since information related to the size of structural changes might be inferred.

Additionally, the complementarity of interferometry at X-band has also been analyzed. Specifically the temporal evolution of the interferometric phase center height might close some of the gaps when having only polarimetric information, as it allows to monitor the plant growth beyond the canopy penetration capabilities and it is also sensitive to the decrease in plant water content during the plant drying and senescence stages, which are not visible with polarimetry at X-band.

7 Literature

[1] V. Akbari, Stian N. Anfinsen, A. P. Doulgeris, T. Eltoft, G. Moser, and S. B. Serpico. Polarimetric SAR change detection with the complex Hotelling–Lawley trace statistic. *IEEE Transactions on Geoscience and Remote Sensing*, 54(7):3953–3966, 2016.

[2] A. Alonso-Gonzalez, T. Jagdhuber, and I. Hajnsek. Exploitation of Agricultural Polarimetric SAR time series with Binary Partition Trees. *Proc. ESA PolInSAR*, 2015.

[3] A. Alonso-González, H. Joerg, K. Papathanassiou, and I. Hajnsek. Dual-polarimetric agricultural change analysis of long baseline TanDEM-X time series data. In *2016 IEEE International Geoscience and Remote Sensing Symposium (IGARSS)*, pages 325–328. IEEE, 2016.

[4] A. Alonso-González, C. López-Martínez, K. P. Papathanassiou, and I. Hajnsek. Polarimetric SAR Time Series Change Analysis Over Agricultural Areas. *IEEE Transactions on Geoscience and Remote Sensing*, 58(10):7317–7330, 2020.

[5] S.R. Cloude and E. Pottier. A review of target decomposition theorems in radar polarimetry. *Geoscience and Remote Sensing, IEEE Transactions on*, 34(2):498–518, 1996.

[6] N.R. Goodman. Statistical analysis based on a certain multivariate complex Gaussian distribution (an introduction). *The Annals of Mathematical Statistics*, 34(1):152–177, 1963.

[7] A. Kostinski and W-M Boerner. On the polarimetric contrast optimization. *Antennas and Propagation, IEEE Transactions on*, 35(8):988–991, Aug 1987.

[8] G. Krieger, A. Moreira, H. Fiedler, I. Hajnsek, M. Werner, M. Younis, and M. Zink. TanDEM-X: A satellite formation for high-resolution SAR interferometry. *IEEE Transactions on Geoscience and Remote Sensing*, 45(11):3317–3341, 2007.

[9] C. Rossi and E. Erten. Paddy-rice monitoring using TanDEM-X. *IEEE Transactions on Geoscience and Remote Sensing*, 53(2):900–910, 2014.